Two-photon electron emission from smooth and rough metal films in the threshold region

Vladimir M. Shalaev,* Constantine Douketis, Tom Haslett, Todd Stuckless, and Martin Moskovits
Department of Chemistry, University of Toronto and Ontario Laser and Lightwave Research Centre, Toronto, Ontario, Canada M5S 1A1

(Received 3 March 1995; revised manuscript received 7 September 1995)

Two-photon photoemission spectra are reported for silver films deposited under ultrahigh vacuum onto a room-temperature (smooth film) or a cold substrate (rough film). A theory is developed which successfully accounts for the qualitative features of the observed spectra in the near-threshold region when the Ag is excited by the absorption of one or two photons. Photoemission from smooth films can be successfully described in terms of direct electron transitions. The traditional one-photon photoemission theory is generalized to include two-photon excitation. Photoemission from rough Ag surfaces is interpreted in terms of the excitation of localized surface plasmons in the roughness features which are assumed to be small polarizable elements of a self-affine fractal. The rapid spatial rate of change in the local electric field surrounding these elements breaks translational invariance, thereby allowing indirect electron transitions to take place, ultimately leading to a predicted (10^3-10^6)-fold enhancement of the two-photon photoemission yield. Approximate analytic expressions are derived for the total photoemission yields following one- or two-photon excitation of smooth silver and two-photon excitation of rough silver.

I. INTRODUCTION

The photoelectron response of metals is known to be enhanced through the excitation of surface plasmons.[1–6] Two varieties of surface plasmons are known: (1) surface plasmon waves (SPW's) and (2) localized surface plasmons (LSP's). SPW's, which propagate laterally along the metal surface, can be optically excited by coupling to an evanescent radiation field,[2,4] or by a field impinging on a grating or on a surface with random roughness.[1] On the other hand, LSP excitation is confined to metal particles or roughness features that are much smaller in size than the wavelength of the incident light. Plasmon oscillations can decay nonradiatively onto one-electron excitations that ultimately yield photoelectrons. This has been discussed in the context of SPW's, where the coupling to electrons occurs through the macroscopic Coulombic fields associated with the SPW's.[1] The decay of bulk (delocalized) plasmons can also be understood in these terms.[7]

The very high local fields in the near zone of the LSP lead to enhanced photoemission which can also be interpreted as nonradiative decay of the LSP into one-electron excitation. In addition, the rapid spatial dependence of the local near-zone fields ($\propto r^{-3}$) breaks the translational invariance of the system and offers a continuous source of momentum. This allows indirect (nonvertical) electron transitions to occur, invalidating the dipole approximation usually invoked in describing optical excitations. LSP excitation is localized in all three directions within the volume of a roughness feature, in contrast with a SPW which is localized in only one dimension, normal to the surface. This greater degree of localization of the electromagnetic energy is the source of the very high local fields associated with the LSP.

It is well known that metal surfaces formed by condensing atomic beams onto a low-temperature substrate are characterized by microscopic surface roughness.[8] Recent evidence suggests that rough metal films are self-affine fractal structures.[9] Such a structure can be simplistically viewed as a fractal cluster of small, interacting metal particles. An assembly of interacting particles each capable of sustaining polar excitation will be characterized by normal modes. When the assembly is a fractal aggregate some of these normal modes have been shown to be strongly spatially localized.[10] Such assemblies of interacting particles capable of sustaining LSP's are known to exhibit a whole range of enhanced optical phenomena[8,11–17] and enhanced surface photochemistry.[18]

Even in the absence of roughness the surface itself breaks translational invariance in the normal direction. The consequence of this symmetry reduction and, in particular, the connection between surface states and nonvertical transitions, is widely discussed in the literature.[19–22] In the pioneering work of Berglund and Spicer experimental data on one-photon photoemission from smooth Cu and Ag films was interpreted in terms of indirect transitions.[23] However, Koyama and Smith showed that those results could be understood in terms of direct transitions alone.[24]

In this paper we generalize the theory of Koyama and Smith to include two-photon photoemission. Expressions are obtained for the distribution of hot electrons and the photoelectron yield in the threshold region. We show that direct transitions are the dominant contributions to the photoemission from smooth films. In contrast, for rough metal films it is the indirect transitions which play the critical role, provided that the surface is excited with photons whose energies lie within the LSP resonance band. It is important to note that these nonvertical transitions do not arise from the trivial symmetry breaking due to the presence of the surface but rather from the rapid spatial rate of change of the near-zone fields associated with the LSP's. Photoemission from rough films excited at a frequency far beyond the LSP resonance band can be successfully describable entirely in terms of direct transitions. Although the theory developed in this paper focuses on a specific experiment, namely, energy-resolved

 © 1996 The American Physical Society

one-photon and two-photon electron emission from rough and smooth Ag surfaces, we believe that it is generally applicable to photoemission at near-threshold energies. The current treatment goes beyond the outline presented previously.[25]

A comparison of the integrated yields for photoemission from smooth and rough Ag films was presented previously.[6] In the present article we report energy-resolved photoemission spectra from rough and smooth Ag and one-photon and two-photon excitation.

The paper is organized as follows. Expressions for the matrix elements responsible for the LSP-induced, nonvertical electron transitions in rough films are presented in Sec. II and compared with those describing direct transitions in smooth films. The theory of two-photon photoemission from metal surfaces is developed in Sec. III. Theories of photoemission from smooth and rough films are presented in Secs. III A and III B, respectively. The experimental apparatus is described in Sec. IV. Experimental results and comparison with the theory are presented in Sec. V.

II. LSP-INDUCED INDIRECT TRANSITIONS

The standard form of the operator, assumed to be a perturbation, describing the effect of the radiative field is

$$\tilde{V}=\frac{e}{2mc}[\tilde{\mathbf{A}}\cdot\mathbf{p}+\mathbf{p}\cdot\tilde{\mathbf{A}}]. \tag{1}$$

Here $\tilde{\mathbf{A}}$ is the vector potential and $\mathbf{p}=-i\hbar\boldsymbol{\nabla}$ is the linear momentum operator. The tilde in (1) indicates the periodic time dependence:

$$\tilde{\mathbf{A}}\equiv Ae^{-i\omega t}+\text{c.c.}\equiv(A^{(0)}/2)e^{-i(\omega t-\mathbf{q}\cdot\mathbf{r})}+\text{c.c.}$$

and

$$\tilde{V}\equiv Ve^{-i\omega t}+\text{c.c.}$$

The classical fields will be chosen so that the macroscopic field amplitude $\mathbf{E}^{(0)}$ inside the film,

$$\tilde{\mathbf{E}}=(\mathbf{E}^{(0)}/2)e^{-i(\omega t-\mathbf{q}\cdot\mathbf{r})}+\text{c.c.},$$

is related to the vector potential amplitude $\mathbf{A}^{(0)}$ by $\mathbf{E}^{(0)}=i\omega\mathbf{A}^{(0)}/c$. We restrict our treatment to near-threshold excitation where the photon energy $\hbar\omega'$ (or the total two-photon excitation energy $2\hbar\omega=\hbar\omega'$) is close to the energy gap $2V_G$ between two conduction bands:

$$|\hbar\omega'-2V_G|\ll\hbar\omega'. \tag{2}$$

Accordingly,

$$\hbar\omega'\sim 2V_G\sim(1/4)\hbar^2G^2\sim E,$$

where E is the electron energy and $\mathbf{G}$ is the reciprocal lattice vector generating the second band.

Let us first consider photoemission from a smooth film. Because the photon momentum of the incident light, $\hbar\mathbf{q}$, is negligible compared to the electron momentum, $\hbar\mathbf{k}$, photoemission will be dominated by direct (vertical) transitions. Consequently the spatial variation of the exciting field may be ignored (dipole approximation). The matrix elements $V\equiv(\mathbf{k}_1|V|\mathbf{k}_2)$ of the interaction operator for transitions between two Bloch states which are nonzero only for direct transitions (i.e., when $\mathbf{k}_1=\mathbf{k}_2$) are approximately given by

$$V_S\sim(e\hbar/m\omega)E^{(0)}k\sim(eE^{(0)}/m\omega)\hbar G \quad \text{if } \Delta\mathbf{k}=0 \tag{3}$$

and $V_S=0$ otherwise. The S subscript indicates that the expression refers to smooth films.

Since the light penetrates hundreds of atomic layers, while translational invariance is broken only for a few atomic layers near the boundary, one anticipates a strong volume, rather than a surface, effect. Accordingly, photoemission in smooth films can be successfully interpreted in terms of direct transitions in the bulk.[24,25]

Analogous expressions for matrix elements appropriate to rough films will now be developed. The surfaces of rough Ag films have been described as a self-affine fractal arrangement of particles that are small with respect to the wavelength of light.[9,26] Because LSP excitation of these roughness features results in greatly enhanced near-zone fields,[8,10–13] photoemission from rough films will be dominated by transitions initiated by the absorption of near-zone (NZ) photons in the vicinity of the roughness features.

The dipolar near-zone field close to a surface roughness feature is given by $E_\alpha^{(\mathrm{NZ})}=E_{\beta'}^{(0)}r^{-3}(\delta_{\alpha\beta}-3n_\alpha n_\beta)\eta_{\beta\beta'}$ where $\mathbf{r}$ is a position vector originating at the center of the roughness feature, $\mathbf{n}=\mathbf{r}/r$, and η is its polarizability. The strong r^{-3} spatial dependence includes Fourier components with high values of $\mathbf{q}^{(\mathrm{NZ})}$, some of which are comparable to $\mathbf{k}$. This breaks translational symmetry and, therefore, eliminates the momentum conservation requirement for optical transitions in metals.

The operator describing the interaction of an electron with near-zone photons is approximately given by

$$V_R\sim(e\hbar/m\omega)E^{(\mathrm{NZ})}\nabla, \tag{4}$$

where

$$E^{(\mathrm{NZ})}\sim(\eta/r^3)E^{(0)}\sim\chi(R_0^3/r^3)E^{(0)}. \tag{5}$$

$\chi\sim\eta/R_0^3$ is the susceptibility associated with the dipolar modes of a roughness feature and R_0 is its mean linear dimension. We assume throughout that R_0 is less than, or of the same order as, the penetration depth (skin depth), R_s, of the light. For rough estimations, we also assume that the excitation of the particles is homogeneous and only dipolar excitations need be considered. Moreover, we will show in Sec. V that excitation of particles with dimensions larger than R_s can be neglected.

The above treatment also makes the simplifying assumption that roughness features are roughly isotropic in shape so that a single linear dimension, R_0, can describe them adequately. One can generalize the analysis somewhat by assuming a collection of spheroids, in which case R_0^3 can be replaced with a^2b (where a and b are the spheroid axes) in the corresponding formula for the polarizability. One can also take into account the so-called lightning rod effect,[8] in cases where the aspect ratio is high, by introducing a susceptibility χ that depends explicitly on the aspect ratio. However, we will show in Appendix B that enhanced photoemission is dominated by structures that are approximately isotropic in shape, and of dimensions of the order of R_s.

Accordingly, little error will be made by assuming that the roughness features are spherical.

An approximate expression for the matrix elements V_R of a rough film is obtained as follows. The wave function describing the electron is assumed to be $\psi \sim v_{\rm loc}^{-1/2} e^{i\mathbf{k}\cdot\mathbf{r}}$, where $v_{\rm loc}$ is the volume within which the electron is localized. We assume further that the photoemission is dominated by contributions from all possible indirect transitions involving resonant intermediate states. Band-structure considerations suggest that the momentum change will be large in this case, so that $|\Delta\mathbf{k}| \sim a^{-1}$ where a is the lattice constant. Under these circumstances the magnitude of the matrix element V_R associated with photoemission from the region of space around a polarized roughness feature of size R_0 is estimated to be

$$V_R(\Delta k \sim a^{-1}) \sim \frac{\eta}{v_{\rm loc}} \frac{e\hbar G}{m\omega} E^{(0)} \int_{R_0}^{\infty} e^{i\Delta\mathbf{k}\cdot\mathbf{r}} r^{-3} d^3r \sim \frac{\eta}{v_{\rm loc}} \left(\frac{a}{R_0}\right)^2 V_S , \tag{6}$$

or, using (5),

$$\frac{V_R(\Delta k \sim a^{-1})}{V_S(\Delta\mathbf{k}=0)} \sim \chi \frac{R_0^3}{v_{\rm loc}} \left(\frac{a}{R_0}\right)^2 . \tag{7}$$

In performing the integration in (6) we assumed that vectors $\Delta\mathbf{k}$ and $\mathbf{r}$ can subtend all angles with equal probability. At resonance, $\chi \sim Q$ where Q is the quality factor of the dipolar resonance. For noble metals $Q \sim 10^2$ and, therefore, the ratio V_R/V_S can be close to unity. For example, for silver with $a = 4$ Å, the ratio (7) will be of the order of unity for surface features with linear dimensions $d = 2R_0 \sim 10^2$ Å if $v_{\rm loc} \sim R_0^3$. The number of all possible indirect transitions is much larger than the number of direct (vertical) transitions. Consequently, one concludes that it is the indirect transitions, made possible by the rapidly varying local fields of the LSP's, that are the dominant contributors to photoemission from rough metal films.

III. THEORY OF TWO-PHOTON PHOTOEMISSION

A. Photoemission from smooth films

The general expression for the electron distribution function $P^{(2p)}(E,\omega)$ per unit time and volume following two-photon excitation is developed in Appendix A, where this distribution function is presented as a sum of two contributions, $P^{(2p)}(E,\omega) = P^{(c)}(E,\omega) + P^{(s)}(E,\omega)$, the first being due to two sequential (cascade) excitations, while the second is due to simultaneous, i.e., true two-photon excitations.

For smooth films, the spatial dependence of the field can be neglected, when the interaction operator is defined within the dipole approximation. For near-threshold excitation, it is the electrons in the vicinity of the ''neck'' of the Fermi surface that are excited and the transitions occur near the L symmetry point: $L_{2'} \rightarrow L_1$. The electronic wave functions near the zone boundary are satisfactorily described by the sum of two plane waves:[27]

$$\psi_1 = a_{11} e^{i\mathbf{k}\cdot\mathbf{r}} + a_{12} e^{i(\mathbf{k}-\mathbf{G})\cdot\mathbf{r}},$$
$$\psi_2 = a_{21} e^{i\mathbf{k}\cdot\mathbf{r}} + a_{22} e^{i(\mathbf{k}-\mathbf{G})\cdot\mathbf{r}}, \tag{8}$$

where

$$a_{11} = (2)^{-1/2}[1 + x^2 - x(1+x^2)^{1/2}]^{-1/2},$$
$$a_{12} = a_{11}[x - (1+x^2)^{1/2}],$$
$$a_{21} = (2)^{-1/2}[1 + x^2 + x(1+x^2)^{1/2}]^{-1/2}, \tag{9}$$
$$a_{22} = a_{21}[x + (1+x^2)^{1/2}],$$
$$x = (\hbar^2/8mV_G) G[G/2 - k_G]. \tag{10}$$

The wave functions in the lower and upper bands are normalized to unit volume and k_G is the projection of the electron momentum on vector $\mathbf{G}$ (or, equivalently, its projection onto the normal to the zone-boundary plane).

The electron energies in the two bands are given by[28]

$$2E_2(\mathbf{k}) = \beta[(\mathbf{k}-\mathbf{G})^2 + \mathbf{k}^2] + \{\beta^2[(\mathbf{k}-\mathbf{G})^2 - \mathbf{k}^2]^2 + 4V_G^2\}^{1/2},$$
$$2E_1(\mathbf{k}) = \beta[(\mathbf{k}-\mathbf{G})^2 + \mathbf{k}^2] - \{\beta^2[(\mathbf{k}-\mathbf{G})^2 - \mathbf{k}^2]^2 + 4V_G^2\}^{1/2}, \tag{11}$$

where $\beta = \hbar^2/2m$.

The surface of constant interband energy is given by

$$E_2(\mathbf{k}) - E_1(\mathbf{k}) - \hbar\omega' = 0,$$

or, using (11), by

$$\beta(G^2 - 2\mathbf{k}\cdot\mathbf{G}) - [(\hbar\omega')^2 - 4V_G^2]^{1/2} = 0. \tag{12}$$

This plane lies parallel to the zone-boundary plane.

Turning specifically to the case of silver, its band structure in the vicinity of the L symmetry line is shown in Fig. 1. At photon energies less than 5 eV this is the only neighborhood in $\mathbf{k}$ space where excitations can occur. The two conduction bands are connected by a direct transition only along the $L\Gamma$ direction when photons of energy 2.43 eV (two-photon case) or 4.85 eV (one-photon case) are used, as in the experiments described below. It is also clear that there are no direct transitions into intermediate states lying between the two conduction bands. The excitation for smooth films in this case occurs via virtual (nonresonant) intermediate states with the same momentum as the initial state. For near-threshold excitation (2) those states lie only in the vicinity of the L_1 and $L_{2'}$ points. We show in Appendix A that the terms $|E_m - E_i - \hbar\omega|$ and $|E_f - E_m - \hbar\omega|$ in (A9) and (A11) can, therefore, be replaced with $\hbar\omega$ to a good degree of approximation.

Since for states with $E_m = E_i + \hbar\omega$ there are no direct transitions, and since the matrix element $V_{im} = 0$, it follows that no sequential two-photon (cascade) electronic excitations occur. That is, $P^{(c)}(E,\omega) = 0$.

The transition matrix elements are obtained as follows. Since the matrix elements are nonzero only for direct transitions, $V_{im}, V_{mf}, V_{m'f}, V_{fm'} \neq 0$ in (A11) only if $E_m, E_{m'} > E_{L_1}$ or $E_m, E_{m'} < E_F$. For the intermediate (one-photon) step in a two-photon excitation, these states are nonresonant and we denote them as f' and i', in order to emphasize that the electron states associated with the

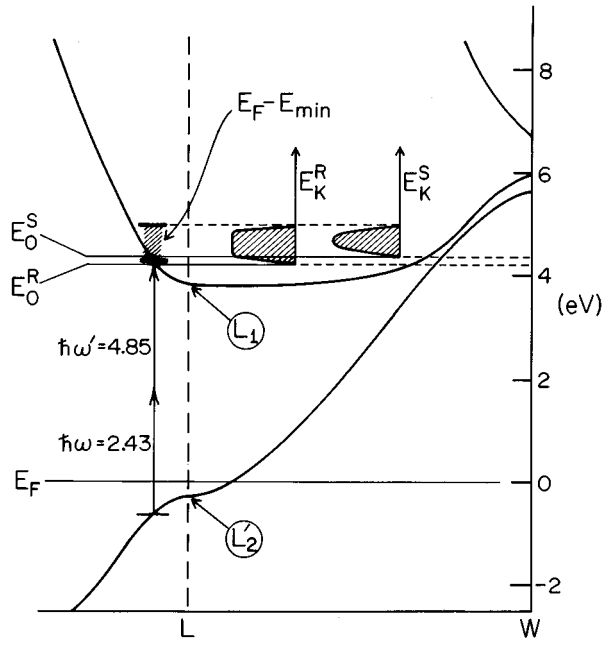

FIG. 1. Band structure of Ag near the L symmetry point. Direct one-photon and two-photon transitions at 4.85 eV total energy are shown. E_0^S and E_0^R mark the vacuum levels of smooth and rough films, respectively, with respect to the Fermi level. Estimated EDC's for rough and smooth films are also shown as arbitrary photoelectron intensities as a function of the outgoing electron kinetic energy $E_K^{R,S}$.

intermediate step of the excitation are positioned in the same energy region as the final states f or the initial states i, respectively. Using (8)–(10) and the equality $\hbar\omega' = 2V_G(1+x^2)^{1/2}$,[27] one gets

$$\langle\psi_1(\mathbf{k})|\nabla|\psi_2(\mathbf{k})\rangle = i(\mathbf{G}/2)(1+x^2)^{-1/2} = i(\mathbf{G}/2)(V_G/\hbar\omega). \tag{13}$$

Note that by assuming excitation near the Brillouin zone boundary (2), $V_G/\hbar\omega \approx 1$, and $k_G \approx G/2$, i.e., $x \ll 1$. For the diagonal element, one finds

$$\langle\psi_2(\mathbf{k})|\nabla|\psi_2(\mathbf{k})\rangle = i\mathbf{k} - i\mathbf{G}a_{22}^2 \approx i(\mathbf{k}-\mathbf{G}/2). \tag{14}$$

Additionally, when only electrons close to the Fermi surface and near the zone boundary are excited one can assume that

$$(\mathbf{k}-\mathbf{G}/2)^2 \approx k_n^2, \tag{15}$$

where $\mathbf{k}_n$ is the radius of the Fermi-surface neck.

Using (1), (3), and (13)–(15), one finds that

$$|V_{if}| \equiv |V_1| = (e\hbar/2m\omega)(V_G/2\hbar\omega)GE^{(0)} \tag{16}$$

for $\mathbf{k}_i = \mathbf{k}_f$. Otherwise it is zero. Likewise

$$|V_{ii'}| = |V_{ff'}| \equiv |V_2| = (eE^{(0)}/2\omega)(2V_n/m)^{1/2} \tag{17}$$

for $\mathbf{k}_f = \mathbf{k}_{f'}$, and zero otherwise. The identity $V_n \equiv (\hbar^2/2m)k_n^2$ was used in (17).

Replacing the summation in the general formula (A11) by an integral, $\Sigma_n \to v(2\pi)^{-3}\int d^3k$, and taking into account that $|P_{im}| = |P_{if'}| \approx |P_{ii'}| \approx \hbar\omega$, because $|E_{f'} - E_i - \hbar\omega| \approx |E_{i'} - E_i - \hbar\omega| \approx \hbar\omega$, (18) may be rewritten in the following form:

$$P^{(s)}(E,\omega) = \frac{4n_G}{\pi^2}\frac{|V_1V_2|^2}{(\hbar\omega)^2}\frac{1}{\hbar}\int' d^3k\,\delta[E_2(k) - E_1(k) - 2\hbar\omega]\,\delta[E - E_2(k)]. \tag{18}$$

Here n_G is the number of symmetry-equivalent lines **G**; and the prime on the integral denotes that the integration is to be performed only over those portions of the **k** space for which $E_1 < E_F$ and $E_2 > E_{L_1}$. One can also convert (18) into a line integral:

$$P^{(s)}(E,\omega) = \frac{4n_G}{\pi^2}\frac{|V_1V_2|^2}{(\hbar\omega)^2}\frac{1}{\hbar}\int' \frac{dl}{|\nabla_k E_2 \times \nabla_k E_1|}. \tag{19}$$

The integral is carried out around the line of intersection of the two surfaces of constant energy $E_2 = E$ and $E_1 = E - 2\hbar\omega$.

For polycrystals one must also average over all values of the angle Θ subtended by **A** and **p** ($|V_1V_2|^2 \propto \cos^4\Theta$; $\langle\cos^4\Theta\rangle_\Theta = \frac{1}{5}$). Using this result and (11), (16), and (17), the integral (19) can be solved to give

$$P_S^{(2p)}(E,\omega) = P^{(s)}(E,\omega) = \frac{n_G}{20\pi}\frac{G}{1-\gamma}\frac{(eE^{(0)})^4}{m\hbar^4\omega^5}\left(\frac{V_G}{\hbar\omega}\right)^2\frac{V_n}{\hbar\omega}, \tag{20}$$

assuming $E_{\min} \leqslant E \leqslant E_F$, and zero otherwise, where

$$E_{\min} = \frac{(2\hbar\omega - \beta G^2)^2 - 4V_G^2}{4\beta G^2}, \quad 1-\gamma = \frac{[(2\hbar\omega)^2 - 4V_G^2]^{1/2}}{2\hbar\omega}. \tag{21}$$

The minimum energy $E_{\min}$ corresponds to the situation where the surfaces $E_1(\mathbf{k}) = E - 2\hbar\omega$ and $E_2(\mathbf{k}) = E$ just touch.[24] The expression for $E_{\min}$ follows from (11) and (12) at $\mathbf{k} = \mathbf{k}_{\min}$ where $\mathbf{k}_{\min}$ is the electron momentum directed along vector **G** so that $\mathbf{k}_{\min}\cdot\mathbf{G} = k_{\min}G$.

The corresponding expression for the one-photon process is

$$P^{(1p)}(E,\omega) = \frac{n_G}{24\pi}\frac{1}{\hbar}\left(\frac{eE^{(0)}}{\hbar\omega'}\right)^2\frac{G}{1-\gamma}\left(\frac{V_G}{\hbar\omega'}\right)^2, \tag{22}$$

which is finite in the range $E_{\min} \leqslant E \leqslant E_F$ and zero otherwise. Accordingly, one-photon and two-photon electron excitations in smooth films lead to rectangular boxlike distributions, $P(E,\omega)$.

The involvement of transitions in the vicinity of the neck of the Fermi surface in near-threshold two-photon processes (14), (15), (17), and (20) is introduced through the matrix elements $V_{ff'}$ and $V_{ii'}$ which are absent in the analogous expression for the probability distribution following one-photon excitation (22), which only involves V_{if}.

It is important to specify the region of validity of these results. To obtain them we used the two-orthogonalized-plane-waves (2-OPW) approximation, and we further assumed that the excitation was in the threshold region. The 2-OPW approximation describes electron transitions between two conduction bands adequately well. It should, therefore,

be an acceptable approximation for silver when the total photon energy lies between approximately 4 and 8 eV. With larger photon energies d-band excitation contributes significantly to the photoemission yield. The threshold requirement (2) is more restrictive. It limits the permissible excitation range for silver to photon energies lying approximately between 4 and 5 eV. In arriving at conclusion (21) regarding the energy range $E_F - E_{\min}$ in which electrons are excited for both one- and two-photon excitation and in obtaining the energy distribution of photoelectrons following one-photon electron excitation, only the 2-OPW approximation was made. Therefore, for silver, these results are valid for excitation with total photon energies in the approximate range 4–8 eV. On the other hand, in obtaining the energy distribution of photoelectrons following two-photon electron excitation (20), we assumed that $P_{im} \approx -i\hbar\omega$ in (A11) and used formula (17) for $V_{ff'} \approx V_{ii'} = V_2$. Both of these results eliminate the dependence on the electron momentum and energy and are based on the requirement that we are near threshold. Accordingly, for silver, the rectangular-box-like form of the energy distribution (20) of photoelectrons following two-photon electron excitation is valid only when the total photon energy $2\hbar\omega$ lies in the range 4–5 eV.

According to the three-step model,[29] the experimentally measured electron distribution curve (EDC) in the threshold region is determined by the product of three factors: (i) $P(E,\omega)$, (ii) the electron transmission function, and (iii) the electron escape function. The electron transmission function, which is essentially a constant over the narrow range of electron energies studied here, has the form[29]

$$t(E) = (nl/R_s)/(1 + nl/R_s), \tag{23}$$

where l is the mean free path for inelastic electron scattering, R_s is the light penetration depth, and $n = 1,2$ for one- and two-photon-excited photoemission, respectively. R_s is related to the absorption coefficient α_a as $R_s = \alpha_a^{-1}$.

The escape function for perfectly free electrons ($E = \beta k^2$) takes the form[29,30]

$$T_S(E) = \frac{1}{2}\left[1 - \left(\frac{E_F + \Phi}{E + \hbar\omega'}\right)^{1/2}\right]. \tag{24}$$

For excitation in the threshold region the modification of the dispersion law due to the presence of the energy gap [Eq. (11)] results in a modified form of the escape function[31] as follows:

$$T_S(E) = \frac{1}{2}\left[1 - \left(\frac{E_F + \Phi - E_{L_1}}{E + \hbar\omega' - E_{L_1}}\right)^{1/2}\right]. \tag{25}$$

In fact, neither of these escape functions describes the electron escape process accurately in the general case. However, in carrying out the calculations below we have decided to use (24) instead of (25) since we speculate that even near the zone boundary quasielastic scattering of the hot electrons redirects most of them along trajectories that are far from the zone boundary. For example, electrons moving along the ΓL symmetry line may be scattered along the LW symmetry line, without loss of energy. The band structure[32] indicates that, in that case, the electron's momentum is far from the zone boundary, suggesting that (24) is the more appropriate function to use here. This quasielastic electron scattering can also result in diffusive electron migration to the surface, resulting in a form of the transmission function that is different from that given in (23).

We have already seen that the distribution of photoexcited electrons is boxlike [(20)–(22)] and that this situation is not changed by the transmission function, which is approximately a constant in the threshold region. Thus the energy dependence of the energy distribution curves is, in this case, almost entirely determined by the escape function. Furthermore, if $E_{\min} + \hbar\omega' < E_F + \Phi$ (this is always the case for Ag, for example) only electrons having energies $E_F + \Phi - \hbar\omega' \leq E \leq E_F$ finally contribute to the photoelectric response, even though electrons in the wider energy range $E_{\min} \leq E \leq E_F$ are excited. The total photoelectric yields, J_1 for one-photon and J_2 for two-photon excitation, defined as the number of photoelectrons per unit time and through unit surface area, are, therefore, given by

$$J_1 = R_s P^{(1p)} tK, \quad J_2 = (R_s/2) P^{(2p)} tK, \tag{26}$$

where

$$K \equiv \int_{E_F + \Phi - \hbar\omega'}^{E_F} T(E)\,dE. \tag{27}$$

It follows from (24), (25), and (27) that in the threshold region K has the form

$$K = \frac{1}{8}\frac{(\hbar\omega' - \Phi)^2}{E_F + \Phi - E_0}, \tag{28}$$

where $E_0 = 0$ when escape function (24) is used and $E_0 = E_{L_1}$ when using (25). Equation (28) is valid when $\hbar\omega' - \Phi \ll E_F + \Phi - E_0$.

Photoemission efficiencies $\eta^{(1p)}$ and $\eta^{(2p)}$ are defined as

$$\eta^{(1p)} \equiv \hbar\omega' J^{(1p)}/I = A_1(\hbar\omega' - \Phi)^2 \tag{29}$$

and

$$\eta^{(2p)} \equiv (\hbar\omega)^2 J^{(2p)}/I^2 = A_2(2\hbar\omega - \Phi)^2, \tag{30}$$

respectively, for one- and two-photon processes, where I is the external radiative intensity. Using (20), (22), (26), and (28) one can show that the photoemission constants A_1 and A_2 are given by

$$A_1 = \frac{n_G}{24} a(\omega') t \frac{GR_s}{1-\gamma} \frac{1}{[\hbar\omega'(E_F + \Phi - E_0)]} \times \frac{e^2}{\hbar c}\left(\frac{V_G}{\hbar\omega'}\right)^2 L(\omega'), \tag{31}$$

$$A_2 = \frac{\pi n_G}{5} a^2(\omega) t \frac{GR_s}{1-\gamma} \frac{1}{[\hbar\omega(E_F + \Phi - E_0)]} \frac{e^4}{m\hbar\omega^2 c^2} \times \left(\frac{V_G}{\hbar\omega}\right)^2 \frac{V_n}{\hbar\omega} L^{(3)}(\omega), \tag{32}$$

where the coefficient a is identically $|E^{(0)}(z=0)|^2/|E_{\text{ext}}^{(0)}|^2$, $E_{\text{ext}}^{(0)}$ being the amplitude of the external field. The coefficient a can be determined from the Fresnel equations (we assume

that the size of irregularities is much smaller than the wavelength). The factors $L(\omega')$ and $L^{(3)}(\omega)$ which account for the Lorentz local field corrections are given by

$$L(\omega')=\left|\frac{\epsilon(\omega')+2}{3}\right|^2 \tag{33}$$

and

$$L^{(3)}(\omega)=\left|\frac{\epsilon(\omega)+2}{3}\right|^4. \tag{34}$$

The photoemission constants are among the quantities that are measured experimentally.

B. Photoemission from rough films

It was shown in Sec. II that the values of the matrix elements for LSP-induced indirect transitions in rough films can be comparable to those for direct transitions [see (7)]. In this case one expects the main contribution to photoemission to be given by transitions executed through resonant intermediate states. If the distribution of intermediate m states is nearly symmetrical in the vicinity of the energy point $E_i+\hbar\omega$, then the value of $|\Sigma_m V_{im}V_{mf}/P_{im}|^2$ in (A11) is given largely by its real part; moreover, for small values of the relaxation constants Γ it may be approximated as

$$|\Sigma_m V_{im}V_{mf}/P_{im}|^2\approx\pi^2[\Sigma_m V_{im}V_{mf}\delta(E_m-E_i-\hbar\omega)]^2. \tag{35}$$

Since the physical quantities discussed here are irrelevant to the initial phases of the matrix elements V_{ij} we have chosen them such that all V_{ij} are real.

Substitution of (35) into (A11) gives

$$P_R^{(s)}(E,\omega)=\left\langle\frac{2\pi^3}{v\hbar}\sum_{if}\left[\sum_m V_{im}V_{mf}\delta(E_m-E_i-\hbar\omega)\right]^2 \times\delta(E_f-E_i-2\hbar\omega)\,\delta(E-E_f)\right\rangle. \tag{36}$$

The angular brackets in (36) indicate averaging over the randomly rough surface, and summation over all roughness features is implied. This includes the averaging over random locations of the polarizable roughness features, which is denoted below as $\langle\cdots\rangle_\chi$, and over their sizes, as $\langle\cdots\rangle_R$. Combining (36) and (A5) and (A10) gives

$$P_R^{(2p)}(E,\omega)=\left\langle\frac{2\pi^2}{v\hbar}\sum_{imf}\left[\frac{2}{\hbar\Gamma_{mm}}+\pi\sum_{m'}\left(\frac{V_{im'}V_{m'f}}{V_{im}V_{mf}}\right)\times\delta(E_{m'}-E_i-\hbar\omega)\right](V_{im}V_{mf})^2 \times\delta(E_m-E_i-\hbar\omega)\,\delta(E_f-E_i-2\hbar\omega) \times\delta(E-E_f)\right\rangle. \tag{37}$$

The first term in the square brackets refers to photoemission resulting from a two-step cascade process; while the second term relates to a two-photon simultaneous excitation process. Using (3), (7), (16), (17), (20), and (21), one obtains the following approximate relations:

$$(1-\gamma)^{-1}(V_1V_2)^2\sim(V_S)^4\sim P_S^{(2p)}G^{-3}\hbar(\hbar\omega)^4 \sim(V_R)^4[\chi(R_0^3/v_{\rm loc})(a/R_0)^2]^{-4}. \tag{38}$$

Assuming that the matrix elements in (37) are constant, and using (38), one then obtains an expression for the enhancement of the optical excitation from rough films as follows:

$$\frac{P_R^{(2p)}(E,\omega)}{P_S^{(2p)}(E,\omega)}\sim\left\langle\left|\frac{a^3}{v}\right|\chi\left(\frac{a}{R_0}\right)^2\frac{R_0^3}{\nu_{\rm loc}}\right|^4 \times(\hbar\omega)^4\left[\frac{2}{\hbar\Gamma_{mm}}+D_m(E_i+\hbar\omega)\right] \times D_i(E_i)D_m(E_i+\hbar\omega)D_f(E_i+2\hbar\omega)\right\rangle. \tag{39}$$

The quantities $D_i(E_i)$, $D_m(E_i+\hbar\omega)$, and $D_f(E_i+2\hbar\omega)$ in (39) are the densities of initial, intermediate, and final states, respectively, in the rough film. The total density of states (DOS) is defined in general as $D(E)=\Sigma_n\delta(E-E_n)$. For electron states localized in roughness features, the DOS is approximated by

$$D\sim a^{-3}v_{\rm loc}E^{-1}. \tag{40}$$

Assuming $v_{\rm loc}\sim R_0^3$, and using (39) and (40), one arrives at the following estimate for the relative propensity for photoelectron emission from rough and smooth films:

$$\frac{P_R^{(2p)}}{P_S^{(2p)}}\sim\left\langle\frac{R_0^3}{v}\left|\chi\right|^4\left(\frac{a}{R_0}\right)^2\left[\frac{2V_G}{\hbar\Gamma_{mm}}+\left(\frac{R_0}{a}\right)^3\right]\right\rangle. \tag{41}$$

The roughness features on the surface are sufficiently closely spaced that electromagnetic resonances sustained by them are strongly coupled. This problem has been solved for a cluster of polarizable particles with fractal character, for which it was shown[12,13] that

$$\langle|\chi|^4\rangle_\chi\sim Q^3, \tag{42}$$

where Q is the quality factor of the resonance, which in the present case is the LSP resonance. The physical meaning of this result is as follows. Strongly disordered collections of interacting dipoles such as random fractal clusters of small polarizable particles possess dipolar eigenmodes which are distributed over a wide spectral range. For fractals, these excitations have been shown to be localized and their spectral distribution to be inhomogeneously broadened.[10,33,34] Hence, the averaged value of a physical quantity over the fractal cluster is approximately given by its value for the particles participating in the resonant eigenmode multiplied by the fraction of the total number of particles which are in resonance. For resonant particles $\chi_{\rm res}\sim Q$, which characterizes the resonant enhancement of local fields due to the excitation of the LSP. Since the fraction of the total number of particles which are resonant is small, the final enchancement $\sim Q^{-1}$ goes as the third power of Q, as in (42).

Rough films are often self-affine[9,26] rather than self-similar. We will assume that the physics of electromagnetic excitation of self-similar fractal clusters outlined above is also valid for self-affine systems so that (42) is approximately applicable.

For structures which scale, the distribution $\rho(R_0)$ as a function of the size of the roughness features will be a power law within the size range $R_{\min}<R_0<R_{\max}$:

$$\rho(R_0)\propto R_0^{-\alpha}. \tag{43}$$

The index α will depend on the fractal dimension D. For specific models of the fractal clusters there exist explicit expressions relating α to D (see Appendix B).

The quality factor of the LSP resonance for small features is approximately given by

$$Q\sim Q_{\text{bulk}}R_0/(R_0+l), \tag{44}$$

where l is the electron mean free path and Q_{bulk} is the resonance quality for the bulk. As the size of the particles decreases electron scattering at their boundary leads to an increase in relaxation rate and, as a result, to a decrease in Q. For very small features, i.e., for $R_0<l$, Q will be approximately proportional to R_0. Formula (44) is valid when the excitation of the roughness features is homogeneous, i.e., when $R_0<R_s$. Contrariwise, we show in Appendix B that when $R_0>R_s$, Q is small. Thus the maximum value of Q is reached at $R_0\sim R_s$.

Averaging in (41) over the polarizabilities of the roughness features [see (42)], and then over their sizes assuming distribution (43), one concludes that it is the roughness features with $R_0\sim R_s$ which contribute predominantly to the photoemission signal. The obtained enhancement of optical excitations for rough films is

$$\frac{P_R^{(2p)}}{P_S^{(2p)}}\sim f(R_s)Q^3(R_s)\left(\frac{a}{R_s}\right)^2\left[\frac{2V_G}{\hbar\Gamma_{mm}}+\left(\frac{R_s}{a}\right)^3\right], \tag{45}$$

where

$$f(R_s)=\langle R_0^3/v\rangle_{R_0}=\frac{1}{v}\int_{R_{\min}}^{R_s}\rho(R_0)R_0^3dR_0 \tag{46}$$

is the volume fraction filled by roughness structures with sizes less than or equal to R_s. When $R_s\sim R_{\max}$ this would correspond to the volume fraction occupied by all of the surface features. To obtain (45) we assumed that we were in the size limit where the mean free path l is larger than R_s,[35] so that $Q\propto R_0$ for $R_0\leqslant R_s$. The volume fraction $f(R)$ depends on the fractal dimension and can be expressed analytically for specific models of rough surfaces (Appendix B).

In the above, we averaged independently over the random positions of the polarizable roughness features and over their sizes. This is not valid in general, and should be considered as an approximation which we believe to be adequate in the context of the estimates that are obtained below.

Formula (45) has a clear physical meaning. The product fQ^3 expresses the enhancement of the excitation due to the high local fields in the vicinity of roughness features. The small term $(a/R_s)^2$, which originates from the Fourier decomposition of the spatial term r^{-3} [Eq. (6)], gives the fraction of the spatial Fourier harmonics with $\Delta k\sim a^{-1}$ that result in resonant nonvertical transitions. The second term in the angular brackets in (45), which normally exceeds the first, expresses the number of the indirect transitions, contributing to the excitation.

Thus, on contrast to surface-enhanced Raman scattering (SERS) where the enhancement is completely determined by the high local fields due to the LSP and is of the order of the third power of the LSP resonance quality,[12,33] photoemission from rough films is determined not only by the high values of the local fields but also by their strong spatial dependence, which leads to indirect electron transitions. The enhancement factor for photoemission, therefore, depends on the parameters of the system in a more complicated manner than that for SERS.

We now consider the escape function $T_R(E)$ for rough films and show it to be different from the corresponding escape function for smooth films, $T_S(E)$. In order for an electron to escape the surface its ''vertical energy,'' $E_v=E_0+\beta k_v^2$, should be larger than the potential barrier $E_F+\Phi$. E_0 is a constant corresponding to the bottom of the energy band for ''hot electrons.'' Elastic scattering of electrons from the boundaries of the roughness features provides a mechanism for reorienting an electron's motion in the proper direction so as to make it contribute to photoemission. This is particularly important in the threshold region.[36] If the electron has total energy $E>E_F+\Phi$ but does not move in a favorable direction ($E_v<E_F+\Phi$), and if the mean free path of the electron in the roughness feature is sufficiently large, repeated bounces at the boundary of the feature will eventually result in an orientation favorable to escape. Thus reflections within the roughness feature offer a means for reorientation of the electron momentum so that ultimately $E_v>E_F+\Phi$.

For spherical particles it was found[36] that the escape function $T_R^{(0)}$ for elastic diffuse, as opposed to specular, reflections has the form

$$T_R^{(0)}(E)=T_S(E)T_t(E)/\{1-[1-T_S(E)]T_t'(E)\}, \tag{47}$$

where

$$T_t(E)=3/2(l/R_0)^4\{2(R_0/l)-3+\exp(-2R_0/l)[2(R_0/l)^2+4(R_0/l)+3]\}, \tag{48}$$

$$T_t'(E)=(l/2R_0)[1-\exp(-2R_0/l)], \tag{49}$$

and $T_S(E)$ is the escape function for the smooth surface [see (24) and (25)]. When $l\gg R_0$, $T_R^{(0)}\approx 1$, i.e., $T_R^{(0)}$ becomes independent of energy E. In the threshold region $T_S\ll T_R$ and thus this mechanism provides an additional enhancement of photoemission entirely through this geometrical factor.

When the reflections at the boundary are specular rather than diffuse, an electron can develop an orientation favorable for escape only if the roughness feature is tapered. The effect of such a tapered geometry can be appreciated if one considers an electron entering a cone with small apical angle Θ. If the initial incidence angle to the boundary is glancing ($\phi_1\approx\pi/2$) so that $E_v<E_F+\Phi$, then after n specular reflections the angle of incidence becomes $\phi_n=\phi_1-(n-1)\Theta$. This formula remains valid until a critical, returning reflection takes place when ϕ_n becomes negative. The smaller the

angle Θ, the closer this critical reflection approaches the normal. Thus the probability for electron escape is also increased as a result of specular reflections.

One should note that, in general, the electron mean free path l occurring in formula (44) is different from that appearing in (47)–(49). In (44) l determines the quality of the plasmon resonance and, is, therefore, sensitive to the changing phase of the collective electron oscillations resulting from collisions. The value of l in (47)–(49), on the other hand, is determined by the cross section for collisions which result in a change in the electron energy. For the sake of simplicity we use the same value for l in the two instances.

The escape function for physically rough surfaces is undoubtedly very complicated. However, it is not unreasonable to assume that the elastic reflections at the boundaries of the roughness features lead to an increased escape probability in the threshold region, thereby weakening the energy dependence of the escape function $T_R(E)$. Likewise, we will assume that there is no need to average the escape probability over the size of the roughness features. Although, in general, the escape probability will depend on the linear size R_0, for features with $R_0 < R_s$ the escape probability is close to unity and there is no need to average.

Let us now consider the total photoelectric yield in the threshold region. It is clear that $T_R(E)$ must equal zero at $E+\hbar\omega' = E_F+\Phi$. Therefore one can assume that for small values of $(E+\hbar\omega'-E_F-\Phi)$ the first nonzero term of the decomposition of $T_R(E)$ gives

$$T_R(E) \propto (E+\hbar\omega'-E_F-\Phi). \tag{50}$$

This result, in particular, follows from (24) and (25) and (47)–(49). It is obvious that the linear dependence which corresponds to the first-order term in an expansion in terms of the detuning $(E+\hbar\omega'-E_F-\Phi)$ is valid in the threshold region for an arbitrary surface. For a small interval of energy near the threshold, one can always neglect the energy dependence of $P(E,\omega)$ and that of the transmission function. It therefore follows from (50) that the total yield is given by the following general expression in the threshold region:

$$J \propto \int_{E_F+\Phi-\hbar\omega'}^{E_F} T(E)dE \propto (\hbar\omega'-\Phi)^2. \tag{51}$$

One arrives, accordingly, at the conclusion that the Fowler expression is a more general law than noted previously. It is not restricted by the assumption of nonconservation of the electron momentum under which it was originally obtained.[30] Moreover, the Fowler law has little to do with the direct or indirect character of electron excitation. Rather, it is a consequence of the linear dependence (50) of the escape function in the threshold region, which is valid generally.[31]

IV. EXPERIMENT

All experiments were carried out in an ultrahigh-vacuum chamber at base pressure 10^{-10} Torr. The chamber is pumped by a 110 l/s turbomolecular pump and a Ti sublimation pump (operating at 300 K) with a conductance of 550 l/s. Ag films were deposited onto a polished Cu substrate with an effusive beam of metal atoms (Ag metal, 99.999%, Johnson Matthey Elect.). The deposition rate was adjusted to give films of about 150 nm thickness within 200 s. This was verified both interferometrically, by observing the appearance of the first fringe in the reflected beam of the 308 nm output of a XeCl excimer laser from the film, and gravimetrically, by measuring the amount of metal deposited onto a calibrated 5 MHz quartz microbalance.

The temperature of the Cu substrate was controlled by connecting the unit to a closed-cycle He refrigerator. An intervening sapphire plate (0.5 mm thick) was used to provide good thermal contact between the substrate and the refrigerator, but with complete electrical isolation. The substrate could be cooled to 30 K in a cool-down time of about 4 h. During operation of the refrigerator the chamber pressure dropped to 7×10^{-11} Torr due to cryopumping.

The surface normal was coincident with the longitudinal axis of an electron time-of-flight tube (2.5 cm i.d. by 1 m long). The mouth of the flight tube was 2 cm from the Cu substrate. The flight tube was shielded from external magnetic fields with two layers of μ metal (Co-netic AA foil) that was routinely demagnetized in both the transverse and longitudinal directions using a smoothly decaying, alternating magnetic field. Although care was taken to eliminate any stray electric fields in the region between the substrate and the flight tube, that region remained magnetically unshielded. Dielectric surfaces in the vacuum chamber, such as viewport glass, were shielded with conductive mesh to eliminate charging problems. Considering the penetration of the earth's field (0.5 G) into the unshielded region, we calculate that the slowest electron which can transverse the flight tube without grounding out against the walls has a kinetic energy of 0.5 eV; this establishes the minimum observable electron kinetic energy in our time-of-flight spectrometer. In order to observe near-threshold photoelectrons, a bias potential, $V_B = +2.00$ V, was applied to the time-of-flight tube. In the observed spectra the low-energy cutoff is given by $\Phi_{S,R}-\Phi_A+V_B$, where $\Phi_{S,R}$ is the work function of the smooth or rough surface where the electrons originate and Φ_A is the work function of the energy-analyzer surfaces where they are detected; the high-energy cutoff is equal to $2\hbar\omega-\Phi_A+V_B$.

Photoelectrons were detected with standard, single-event counting techniques. Electrons arriving at the end of the flight tube exit the drift region through a grounded grid and are accelerated toward a microchannel plate detector (Galileo FTD-2003) by an electrostatic potential of 300 V. The output is impedance matched to the 50 Ω input of a digital oscilloscope (LeCroy 9400), which was interfaced to a personal computer. Typical electron arrival rates of a few counts per second were used. Higher count rates resulted in space-charge-distorted spectra. Time-to-kinetic-energy conversion was achieved using a cubic weighting factor. No smoothing was performed on any of the data presented here.

The laser system consists of a XeCl excimer laser pumping a dye laser with frequency-doubling capability (Lumonics Ex-520, HD-300, HT-1000). Coumarin-500 dye (Exciton) and a KB5 crystal provided radiation at 2.43 eV (510 nm) and 4.85 eV (255 nm), respectively. The dye laser power was kept below 0.5 μJ/pulse for rough films, and below 20 μJ/pulse for smooth films to prevent space-charge effects.[37] The second-harmonic light power was severely attenuated to give low electron count rates. The laser light

impinged on the Cu substrate at a 35° incidence angle with respect to the surface normal. The light passed through two high-extinction linear polarizers adjusted to provide a common state of polarization for both visible and uv laser beams. Then the beams were focused onto the substrate with a simple fused silica lens (focal length 20 cm). We measured a near-Gaussian spatial profile at the focal point of 0.3 mm half width at half maximum (HWHM). Based on a calculation using well-known optical constants for Ag (Ref. 38) the penetration depth at 35° incidence angle is 124 Å at 510 nm and 140 Å at 255 nm. Under these fluence conditions, we calculate that local heating of the surface during the pulse increases the temperature by only 10 K; annealing of the prepared rough film was not observed even after extended periods of irradiation. The temporal profile of the laser was found to be Gaussian with 7.1 ns HWHM. This value, together with the time response of the detector and signal analyzer, added in quadrature, results in an overall time resolution of 19 ns. Using these parameters the experimental energy resolution of our spectrometer is given by $\Delta E = 0.023 E^{3/2}$ (with E in units of eV).

Photoelectron spectra of smooth Ag films were recorded at room temperature immediately after deposition and at 30 K after the 4 h cool-down time. During this 4 h period photoelectron spectra were recorded approximately every 30 min so that work function changes could be noted. Some smooth film surfaces were dosed with H_2O to reduce Φ_S and thereby increase the range of the energy window within which the photoelectric signal appears. Only the low-energy cutoff shifts on dosing; the high-energy cutoff remains fixed, indicating that Φ_A is not affected. Stepwise dosing with H_2O to a total of 5 L reduced the low-energy cutoff by 0.6 eV, beyond which no further change was observed. H_2O does not have any electronically excited states that are accessible with our laser light, the nearest one being 7.5 eV above the ground state of the molecule. Photoelectron spectra of rough Ag films were recorded at 30 K immediately after deposition.

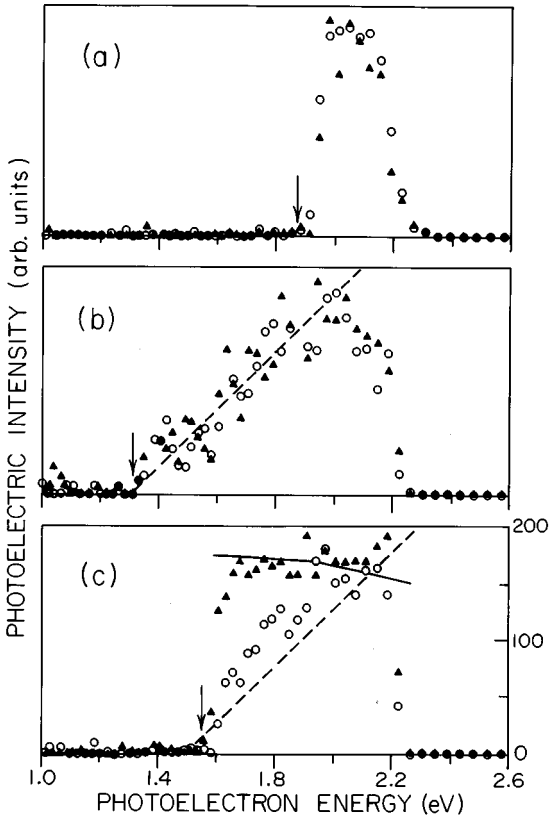

FIG. 2. Normalized two-photon (triangles) and one-photon (circles) photoemission spectra for (a) a smooth Ag film at room temperature, (b) a smooth film at 30 K dosed with 5 L H_2O, and (c) a rough film at 30 K. The dashed lines in (b) and (c) indicate the form of the electron transmission function $T_S(E)$. The scale on the right-hand side refers to the DOS product, discussed in the text, in units of $\mathrm{Ry}^{-3}\,\mathrm{atom}^{-3}$. The total photon energy $\hbar\omega' = 2\hbar\omega = 4.85$ eV. The upper and lower energy cutoffs are determined by $E_{\mathrm{upper}} = (2)\hbar\omega - \Phi_A + V_B$ and $E_{\mathrm{lower}} = \Phi_{S,R} - \Phi_A + V_B$. The differing values of E_{lower} (arrows) are due to variations in $\Phi_{S,R}$.

V. RESULTS AND DISCUSSION

Normalized one-photon and two-photon spectra of a smooth film at room temperature, of a smooth film at 30 K dosed with 5 L H_2O, and of a rough film at 30 K are shown in Fig. 2. The one-photon and two-photon spectra are distinguished by the shape of the points. For a smooth film [Fig. 2(a)] the one- and two-photon spectra are identical to within the signal-to-noise level. This observation is consistent with theory: for both two-photon and one-photon excitation in smooth films, the probabilities of excitation as a function of energy [(20)–(22)] have a boxlike form.

The EDC is determined by the product of the rectangular $P(E,\omega)$ function with the $T_S(E)$ function which is essentially triangular over the narrow energy range utilized in these experiments. The influence of $T_S(E)$ is not apparent in Fig. 2(a) because of the very narrow range width of the spectrum. In Fig. 2(b), where this range is extended through the lowering of Φ_S, $T_S(E)$ is shown as a dashed line. The overall photoelectron spectrum fits this curve well, implying that the EDC is, indeed, a product of a boxlike $P(E,\omega)$ and a triangular $T_S(E)$. The good agreement with theory also implies that both one-photon and simultaneous two-photon photoemission from smooth films are initiated by direct transitions in the bulk.

The above conclusion is not unexpected, at least not in the one-photon case, since no one-electron transitions are observed in the absorption spectrum of Ag below the plasma edge at approximately 3.8 eV.[38] (The weak absorption of Ag in the visible is due to collective excitations described by the Drude formula.) Photoemission induced by the excitation of Drude electrons is known to be polarization sensitive[39] even after factoring out the small polarization dependence due to the differing Fresnel reflectivities[40] for s- and p-polarized light. We observe no such polarization dependence, corroborating further our conclusions that the transitions are direct.

The one-photon and two-photon spectra of a rough Ag film, shown in Fig. 2(c) are strikingly different from those of the smooth films. The one-photon spectrum is largely triangular in shape and resembles the smooth film EDC's, although there is a small positive deviation from the triangular shape that is clearly evident. The two-photon spectrum is distinctly rectangular; these results were reproduced with many films of varying thickness. The sharp increase within a

narrow energy interval, ~ 0.1 eV, at the left edge of the spectrum corresponds to the range where the Fowler law is valid (see below). (The spectrum is found to be only weakly dependent on the presence of adsorbate molecules and is independent of the light polarization.) These spectra can be understood by assuming that the one-photon response in rough films is due largely to direct transitions while the two-photon response originates from LSP-mediated, indirect transitions.

The high local fields of the LSP's also enhance the excitation of electrons by direct transitions. The corresponding probability of excitation is given by

$$\frac{P^{(2p)}_{R,\text{direct}}}{P^{(2p)}_{S}} \sim f(R_s)Q^3(R_s). \tag{52}$$

Comparing (52) and (45) one finds

$$\frac{P^{(2p)}_{R}}{P^{(2p)}_{R,\text{direct}}} \sim \frac{R_s}{a} + \frac{2V_G}{\hbar\Gamma_{mm}}\left(\frac{a}{R_s}\right)^2 \gg 1. \tag{53}$$

The second term in (53) may be larger than, of the order of, or less than unity; however, the first term is always much larger than unity and thus (53) holds. This supports the conclusion regarding the dominance of the LSP-induced indirect transitions in the photoemission.

The enhancement factor for rough films can now be estimated. Assuming $R_s \approx 100$ Å (for bulk Ag, the penetration depth at 35° incidence is 124 Å at 510 nm and $l \approx 400$ Å,[35] one finds from (44) that the quality factor for the LSP resonance, $Q \approx 24$ so that $Q^3 \approx 10^4$. (For a disordered Ag film the optical penetration depth may be larger; however, this does not alter our estimates seriously.) The lattice constant a for Ag is 4 Å, $(R_s/a)^3 \sim 10^4$. Hence $2V_G/\hbar\Gamma_{mm}$ can have approximate values in the range 10^2 to 10^4, depending on the value of the lifetime $(\Gamma_{mm})^{-1}$. Accordingly, $(R_s/a)^3 \geqslant 2V_G/\hbar\Gamma_{mm}$ in (45). Using these values, and $f(R_s) \sim 10^{-3}$–10^{-1} (see Appendix B for the rationale), in (45) one obtains the following estimate for the enhancement of the optical excitations in rough films:

$$\frac{P^{(2p)}_{R}}{P^{(2p)}_{S}} \sim 10^2 - 10^4. \tag{54}$$

The enhancement factor G for photoemission includes an additional contribution associated with the enhanced escape probability T_R from the roughness features as compared to its counterpart T_S for smooth films. Thus,

$$G \sim (T_R/T_S)(P^{(2p)}_{R}/P^{(2p)}_{S}). \tag{55}$$

The maximum value of $T_R \approx 1$ is reached when $l \gg R_0$. In that case, the factor (T_R/T_S) is approximately equal to T_S^{-1} which can be much larger than unity in the threshold range. Assuming (T_R/T_S) to lie in the range 10–10^2,[36] one ultimately obtains from (54) and (55)

$$G \sim 10^3 - 10^6. \tag{56}$$

The experimentally observed enhancement of 2000–3000 previously reported by us[6] lies within this range.

We are now in the position to calculate photoemission cross sections for both one- and two-photon-excited photoemission and to compare them with experimentally measured values. Using literature values of ϵ for Ag,[38] and (23), (33), and (34), one obtains $t(\omega') \approx 0.7$, $t(\omega) \approx 0.9$, $L(\omega') \approx 2.1$, and $L^{(3)}(\omega) \approx 180$. From the Fresnel formulas,[40] one gets $a(\omega') \approx 0.4$ and $a^2(\omega) \approx 0.1$ for p-polarized light and angle of incidence $\Theta = 45°$. Taking E_0 to equal 0 in (31) and (32) [see the discussion following Eq. (25)] and using the parameter values $E_F = 5$ eV, $G = 2.8\times 10^8$ cm^{-1}, $2V_G = 4.2$ eV, and $\Phi = 4.3$ eV,[24] one ultimately obtains $A_1 \approx 7\times 10^{-3}$ electron/photon eV^2 and $A_2 \approx 2\times 10^{-33}$ electron cm^2 s/photon^2 eV^2. This is in reasonable agreement with the experimentally measured values $A_1 = 2.3\times 10^{-4}$ and $A_2 = 1.1\times 10^{-33}$.[6] In view of the simplifications made in order to obtain analytic expressions, and of the remaining uncertainty regarding the form of the transmission and escape functions, this level of agreement for so great a range of processes is quite satisfactory and implies that the essential physics is explained properly by our approach.

We showed previously that the electron excitation probability $P(E,\omega)$ is determined by the product $D_i(E)D_m(E+\hbar\omega)\ D_f(E+2\hbar\omega)$ for sequential two-step excitation and $D_i(E)[D_m(E+\hbar\omega)]^2 D_f(E+2\hbar\omega)$ for a simultaneous two-photon process [see (39)]. The additional contribution from the intermediate density of states for the simultaneous two-photon process reflects the interference character of this excitation. Within the narrow energy interval studied here, the density of states for Ag is essentially independent of energy[32] so that both products should ultimately lead to a rectangular-box-like distribution. If the two-photon simultaneous process dominates the two-step process, then $P^{(2p)}(E,\omega)$ is proportional to $D_i(E)[D_m(E+\hbar\omega)]^2 D_f(E+2\hbar\omega)$.

The solid line in Fig. 2(c) represents this product of the densities of states for Ag.[41] One can see that the energy dependence of $P^{(2p)}_R(E,\omega)$ is negligible in this case.

It was shown at the end of Sec. III that the escape function appropriate for rough films is a weaker function of energy than the corresponding function for smooth films. In the limit where the electron mean free path is much larger than the size of the roughness features, the escape probability is expected to equal unity independent of energy. The fact that the form of the EDC shown in Fig. 2(c) is rectangular rather than triangular implies that in this case essentially all of the photoelectrons originate from the roughness features.

The nearly triangular one-photon response in Fig. 2(c) implies that the surface features which are the main contributors to one-photon photoemission are typically larger in size than those which are the predominant contributors to the LSP-mediated two-photon photoemission; this implies that elastic reflections at the boundaries of the roughness features are not important in one-photon photoemission. This is consistent with the conclusions developed above that LSP excitation, and hence LSP-mediated two-photon photoemission, originate predominantly in features with $R_0 \sim R_s$. In contrast, for one-photon excitation with $\hbar\omega' = 4.85$ eV, LSP's are not excited and photoemission resulting from excitation of electrons within roughness features of size R is simply proportional to the volume fraction $f(R) \sim (R/R_c)^{3-\alpha}$, which increases with increasing size of the feature. Accordingly, one expects the main contribution to one-photon photoemission to be due to structures with sizes comparable to

or larger than the mean free path l, reducing the importance of the effect of reflections at the features' boundaries. The corresponding escape function and the EDC should, and do, resemble the analogous quantities for smooth films but the EDC has a small, positive deviation.

The LSP excitation in rough films is only observed with visible photons. This is consistent with the report of an anomalous visible absorption in roughened Ag,[14,42] which has been ascribed to surface plasmon excitations.[14,42]

The photoemission spectra of the rough films are not affected by the polarization of the laser, apart from the trivial Fresnel reflectivity effect. This is entirely consistent with LSP excitation in surface roughness features and is well known in other phenomena, for example, SERS.[8]

The difference between the two spectra of Fig. 2(c) might also be explained in terms of roughness-induced surface states. However, surface states are expected to be strongly polarization dependent and very sensitive to surface contamination:[19,20] neither is observed here. Furthermore, electron energy loss studies[43] and inverse photoemission measurements comparing rough and smooth[44] Ag show no evidence of surface states. Both studies suggest that the bulk electronic structure of rough and smooth Ag films is very similar. Our results support that conclusion.

We have previously reported two-photon-induced photoemission spectra excited with a XeCl excimer laser ($\hbar\omega = 4$ eV).[45] Excitation with photons of that energy allowed us to investigate a wider energy interval of photoelectrons. (No bias potential was needed for those experiments.) At photon energies far beyond the LSP resonances the excitation should occur via direct transitions. Consequently, electron excitation is expected to occur in the same energy interval for both rough and smooth films. The majority of photoelectrons registered in that experiment had energies between 1.3 and 3.3 eV so that the corresponding energy interval of excited electrons is $\Delta E = 2$ eV for both rough and smooth films. This is in good agreement with the value for $E_F - E_{\min}$ calculated using (21) together with the values for the other parameters used above. The low-level background of photoelectrons extending to energies lower than 1.3 eV reported in Ref. 45 is due to secondary electrons emitted from the time-of-flight tube. The EDC's obtained in that experiment[45] had neither rectangular nor triangular forms. This is not in contradiction with the present theory, which only applies in the near-threshold region which for Ag is restricted to total photon energies below 5 eV. However, the theory is more robust regarding the energy interval $E_F - E_{\min}$ in which electrons are excitable. In this respect, the theory applies up to a total photon energy of approximately 8 eV, and, indeed, it appears to account successfully for the experimentally observed width of the EDC obtained with (twice) 4 eV, two-photon excitation.

The lower EDC cutoff energies are indicated by vertical arrows in Figs. 2(a), 2(b), and 2(c). The upper energy cutoff comes at approximately the same energy (~ 2.2 V) for all of the spectra shown in Fig. 2, as it should, since it depends only on constant instrumental parameters. The width of an observed photoelectron spectrum is sometimes smaller than $E_F - E_{\min}$ [cf. Fig. 2(a)]. In fact, it is determined by the smaller of two quantities. One is the difference between the maximum and the minimum electron energies required by

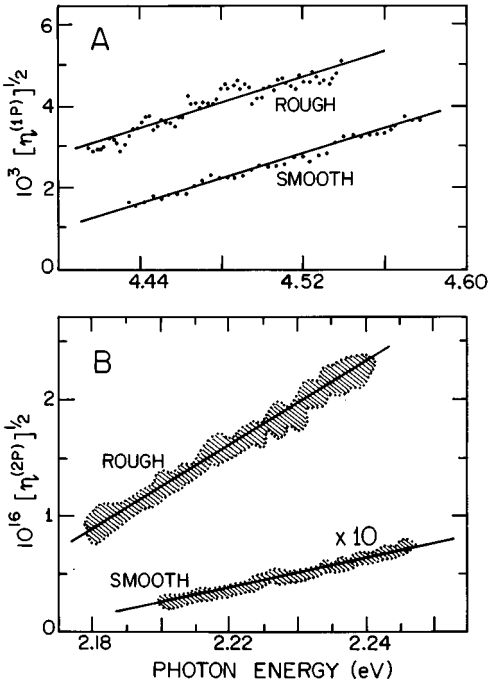

FIG. 3. Fowler plots for rough and smooth Ag films (square root of the quantum yield as a function of photon energy) for (A) one-photon and (B) two-photon photoemission. The shaded areas in (B) contain hundreds of points. Note that the smooth-film data in (B) have been expanded by an order of magnitude to quantitatively reveal the slope.

energy conservation. This is equal to $(2)\hbar\omega - \Phi_{S,R}$ where $\Phi_{S,R}$ is the work function of the smooth or rough surface. The other is the value of $\Delta E = E_F - E_{\min}$ as defined previously. When $\Delta E < (2)\hbar\omega - \Phi_{S,R}$ it is ΔE which restricts the width. Otherwise $(2)\hbar\omega - \Phi_{S,R}$ does. The former quantity (ΔE) was previously estimated to be ~ 0.7 eV.[25] It is clear from Fig. 2 that its actual value is somewhat larger than this, so that the widths of the photoemission spectra of silver excited with visible light are limited by the condition $(2)\hbar\omega - \Phi_{S,R}$. The variation of the low-energy cutoffs in Fig. 2 is, therefore, almost entirely determined by the differing values of the work functions of the surfaces involved. The smooth film has the largest value of Φ and the water-covered smooth film the lowest. In contrast to this, when silver is excited with two 4.0 eV photons, the photoemission spectral width was limited by $E_F - E_{\min}$. (The width would have been of the order of 3.8 eV had energy conservation been the limiting factor.)

Figure 3 indicates that one-photon photoemission from rough films is only slightly enhanced over that of a smooth film when the LSP is not excited. This small enhancement can be easily accounted for in terms of the increased surface area for the rough film. In contrast, LSP-mediated two-photon photoemission from rough films is larger by some three orders of magnitude than that from smooth films. This accords well with the theory presented above.

The discussion regarding the applicability of the Fowler formula, which was an amplification of material reported in Ref. 31, is also confirmed experimentally. Figure 3 presents Fowler plots for one-photon ($\hbar\omega' = 4.5$ eV) and two-photon

($\hbar\omega = 2.2$ eV) photoemission from cold-deposited (rough) and warm-deposited (smooth) films.[6] The quadratic dependence on the energy excess between the photon energy and the work function is found to hold very well within the narrow energy interval ~ 0.1 eV near the photoemission threshold, for one- and two-photon excitation and for both rough and smooth films. This implies that the Fowler relation is independent of the character of the electron excitation, which is direct in the case of smooth films and also in the case of rough films excited with photons with energies lying beyond the LSP resonance band, and indirect for rough films excited within the LSP band. This experimental observation supports the conclusion that the Fowler law is valid to a more general extent[31] than that expressed in its original formulation.[30]

To conclude, we have presented an approximate theory of photoemission pertinent to near-threshold excitation following one- and two-photon absorption by rough and smooth films. The rough films are assumed to be adequately described by a self-affine structure. The theory was tested by recording the time-of-flight photoemission spectra of rough and smooth Ag films prepared under UHV conditions. The basic ideas of the theory are as follows. Photoemission takes place via direct optical transitions except under circumstances where LSP modes are activated. Strongly enhanced photoemission is then dominated by excitation from the near-zone fields around surface roughness features, and the escape of hot electrons takes place with little dependence on electron energy. The breaking of translational invariance allowing these indirect transitions to occur results from the rapidly varying spatial dependence of the intense local fields accompanying the LSP excitation. The experimental results are in good qualitative agreement with the theory. Additionally, estimates of the photoemission cross sections based on the theory are in fair accord with measurements.

ACKNOWLEDGMENTS

We are grateful to NSERC and CEMAID for financial support. Work at NMSU was supported in part by NSF under Grant No. DMR-9500258. We thank Dr. Valery Smelyansky for providing us with unpublished density-of-states calculations for silver.

APPENDIX A

The equation of motion of the one-electron density matrix ρ is given by

$$(d/dt+\Gamma)\rho = -i/\hbar[H,\rho], \tag{A1}$$

where the full Hamiltonian H is a sum of the Hamiltonian of the system in the absence of radiation, H_0, and the perturbation V, and Γ is the relaxation operator. Solving the system of equations for matrix elements $\rho_{nn'}$ $(n,n'=i,m,f)$ to fourth order in the steady regime, one finds that

$$\Gamma_{ff}\rho_{ff} = \frac{2}{\hbar}\mathrm{Re}\sum_{im'm}\frac{V_{im}V_{mf}V_{m'i}V_{fm'}}{P_{im}P_{if}P_{m'f}} + \frac{4}{\hbar^2\Gamma_{mm}}\mathrm{Re}\left[\sum_m \frac{V_{fm}V_{mf}}{P_{mf}}\right]\mathrm{Re}\left[\sum_i \frac{V_{im}V_{mi}}{P_{im}}\right], \tag{A2}$$

where

$$P_{im} = \hbar\Gamma_{im} + i[\hbar\omega - E_m + E_i],$$
$$P_{mf} = \hbar\Gamma_{mf} + i[\hbar\omega - E_f + E_m], \tag{A3}$$
$$P_{if} = \hbar\Gamma_{if} + i[2\hbar\omega - E_f + E_i].$$

The subscripts i, m, and f refer to initial, intermediate, and final states with energies $E_i \leqslant E_F$, $E_F < E_m < E_{L_1}$, and $E_f \geqslant E_{L_2}$, respectively, E_F is the Fermi level energy, and E_{L_1} is the lowest energy in the second conduction band. The diagonal matrix element ρ_{ff} represents the probability of observing an electron in state f, and the term $\Gamma_{ff}\rho_{ff}$ represents the corresponding steady-state probability per unit time of excitation into state f.

The electron energy distribution $P^{(2p)}(E,\omega)$ per unit time and unit volume following two-photon excitation is defined as

$$P^{(2p)}(E,\omega) = v^{-1}\sum_f \Gamma_{ff}\rho_{ff}\delta(E-E_f), \tag{A4}$$

where v is the sample volume. Substituting (A2) into (A4), one obtains

$$P^{(2p)}(E,\omega) = P^{(c)}(E,\omega) + P^{(s)}(E,\omega), \tag{A5}$$

where

$$P^{(c)}(E,\omega) = \frac{4}{\hbar^2 v}\sum_{imf}\frac{1}{\Gamma_{mm}}\mathrm{Re}\left[\frac{V_{im}V_{mi}}{P_{mi}}\right]\mathrm{Re}\left[\frac{V_{fm}V_{mf}}{P_{mf}}\right]\delta(E-E_f) \tag{A6}$$

and

$$P^{(s)}(E,\omega) = \frac{2}{\hbar v}\sum_{imm'f}\mathrm{Re}\left[\frac{V_{im}V_{mf}V_{fm'}V_{m'i}}{P_{im}P_{if}P_{m'f}}\right]\delta(E-E_f). \tag{A7}$$

The term $P^{(c)}$, which is proportional to the lifetime Γ_{mm}^{-1} in the intermediate state, expresses the contribution of two sequential (cascade) excitations to the photoemission; the term $P^{(s)}$, on the other hand, describes the contribution of simultaneous, i.e., truly two-photon excitation processes.

The relaxation constants Γ are much smaller than the characteristic frequency ω. This allows us to replace the resonant factors $\mathrm{Re}[P_{ij}^{-1}]$ by δ functions; hence

$$P^{(c)}(E,\omega) = \frac{(2\pi)^2}{v\hbar}\sum_{imf}\frac{|V_{im}V_{mf}|^2}{\hbar\Gamma_{mm}}\delta(E_m - E_i - \hbar\omega) \times \delta(E_f - E_m - \hbar\omega)\,\delta(E-E_f) \tag{A8}$$

and

$$P^{(s)}(E,\omega)=\frac{2\pi}{v\hbar}\sum_{imm'f}\mathrm{Re}\left[\frac{V_{im}V_{mf}V_{fm'}V_{m'i}}{P_{im}P_{m'f}}\right]\times\delta(E_f-E_i-2\hbar\omega)\,\delta(E-E_f). \quad \text{(A9)}$$

Since $E_m=E_i+\hbar\omega$ and, accordingly, $E_f-E_m-\hbar\omega=E_f-E_i-2\hbar\omega$, one can rewrite (A8) as

$$P^{(c)}(E,\omega)=\frac{(2\pi)^2}{v\hbar^2}\sum_{imf}\frac{|V_{im}V_{mf}|^2}{\Gamma_{mm}}\delta(E_m-E_i-\hbar\omega)\times\delta(E_f-E_i-2\hbar\omega)\,\delta(E-E_f). \quad \text{(A10)}$$

Since $E_i+2\hbar\omega=E_f$ it also follows that $P_{m'f}\approx P^*_{im'}$ so that (A9) becomes

$$P^{(s)}(E,\omega)=\frac{2\pi}{v\hbar}\sum_{if}\left|\sum_m\frac{V_{im}V_{mf}}{P_{im}}\right|^2\delta(E_f-E_i-2\hbar\omega)\times\delta(E-E_f). \quad \text{(A11)}$$

Note that since there is no resonance with virtual intermediate states for direct two-photon excitations ($P_{im}\approx-\hbar\omega$), we have not replaced the term $|P_{im}^{-1}|$ in (A9) and (A11) with δ functions. Expressions (A10) and (A11) form the basis of the analysis for photoemission from rough and smooth films.

APPENDIX B

For certain specific disordered systems the functions $\rho(R_0)$ and $f(R_s)$ [(43) and (46)] and many of the other expressions discussed above maybe expressible in closed form. It is instructive to consider one of these in some detail since it will provide a better sense of the acceptability of the various approximations made. For a Brownian surface,[46] any vertical section through the surface generates a curve characteristic of Brownian motion. The surface $Z(x,y)$ satisfies the scaling relation

$$Z(\lambda x,\lambda y)=\lambda^H Z(x,y) \quad \text{(B1)}$$

for any value of λ, and codimension $H=3-D$. The fractal dimension D for the Brownian surface is $D_s=2.5$ and $H=0.5$. The scaling relation (B1) applies to a fractal surface which is self-affine rather than self-similar.

For every pair of points $\mathbf{r}'$ and $\mathbf{r}''$ on the Brownian surface $[Z(\mathbf{r}')-Z(\mathbf{r}'')]^2\propto r^{2H}$ where r is the distance between the points. Mandelbrot used this formula to generalize the Brownian surface with $H=0.5$ to a fractional Brownian surface by assuming that H can have an arbitrary value between 0 and 1.[46] This allows one to define self-affine fractal surfaces with an arbitrary fractal dimension $D_s=3-H$ ranging between 2 and 3. Fractional Brownian surfaces are reminiscent of a natural landscape.

To some extent, one may envision the interaction of the light with the rough surface as the excitation of ''islands'' with average height of the order of R_s. Since the light penetrates the rough sample in an exponentially decreasing fashion characterized by a penetration depth, the problem corresponds approximately to one in which light interacts with disordered material above a base plane. The intersection of this base plane with the fractal surface defined above results in a ''landscape'' consisting of islands and coastlines. The fractal dimension of these coastlines is $D=2-H=1.5$.[46,47] Therefore modeling the problem of the interaction of light with a self-affine fractal object in terms of a system in which light interacts with islands of dimension R_s is not an unreasonable approach. These islands satisfy the Korcak distribution:[46]

$$Nr(A>a)\sim a^{-D/2}, \quad \text{(B2)}$$

where $Nr(A>a)$ is the number of islands having a projected area A greater than a prescribed value a. Mandelbrot showed that (B2) is valid for arbitrary fractional Brownian surfaces. Since the linear size along the x and y axes is, on average, the same, one can rewrite (B2) in terms of linear size R:

$$Nr(R>R_0)=\int_{R_0}^{R_{\max}}\rho(R_0)dR_0\propto R_0^{-D}. \quad \text{(B3)}$$

It follows from (43) and (B3) that α introduced in (43) can be expressed in terms of D as

$$\alpha=D+1. \quad \text{(B4)}$$

In particular, $\alpha=D_s=2.5$ for the regular Brownian surface.

Islands with transverse dimensions R_0 significantly larger than R_s can be approximately regarded as high-aspect-ratio, oblate spheroids. Since $R_0\gg R_s$, only the axially symmetrical dipole mode is excited in this case. The resonant frequency of this mode for an oblate spheroid is shifted to shorter wavelengths and for metals has a low optical quality of resonance ($Q\sim1$).[48] Since the efficiency of two-photon excitation is proportional to Q^3 [see (45)] it is clear that the contribution of oblate islands with transverse size $R_0\gg R_s$ to the excitation can be neglected.

On the other hand, it follows from (41)–(45) and (B4) that the probability of two-photon excitation, as given by (41), is a rapidly increasing function of the size R_0, when $R_0<R_s$. Therefore, in accordance with (45), one concludes that the contribution of prolate spheroids with $R_0\ll R_s$ can also be neglected, so that the major contribution to the LSP-mediated two-photon electron excitation is due to roughness features of size $R_0\sim R_s$, approximately equal in all three dimensions.

An approximate expression for the volume fraction $f(R_s)$ of a Brownian surface can also be derived. For real rough surfaces there is a correlation radius R_c, within which the scaling property occurs. For larger dimensions the rough surface can be considered as trivial mixture of clusters of size R_c embedded in a medium. Accordingly, using (43) and (46), one obtains

$$f(R_s)\sim(R_s^3/R_c^2R_s)(R_c/R_s)^{\alpha-1}\sim(R_s/R_c)^{3-\alpha}. \quad \text{(B5)}$$

For a Brownian surface with $R_c\sim1$ μm and $R_s\sim10^2$ Å, $f(R_s)\sim10^{-1}$. For smaller values of D and $R_c\sim10$ μm, $f(R_s)$ can be as small as 10^{-3}.

*Permanent address: Physics Department, New Mexico State University, Las Cruces, NM 88003.
[1] J. G. Endriz and W. E. Spicer, Phys. Rev. Lett. **24**, 64 (1970); Phys. Rev. B **4**, 4159 (1971).
[2] H. W. Rudolf and W. Steinmann, Phys. Lett. **61A**, 471 (1977).
[3] U. Even, K. A. Holcomb, C. W. Snyder, P. R. Antoniewicz, and J. C. Thompson, Surf. Sci. **165**, 35 (1986).
[4] T. Tsang, T. Srinivasan-Rao, and J. Fisher, Opt. Lett. **15**, 866 (1990).
[5] W. Drube and F. J. Himpsel, Phys. Rev. Lett. **60**, 140 (1988).
[6] J. T. Stuckless and M. Moskovits, Phys. Rev. B **40**, 9997 (1989).
[7] J. Hofmann and W. Steinmann, Phys. Status Solidi **30**, K53 (1968).
[8] M. Moskovits, Rev. Mod. Phys. **57**, 783 (1985).
[9] R. Chiarello, V. Panella, J. Krim, and C. Thompson, Phys. Rev. Lett. **67**, 3408 (1991); J. Krim, I. Heyvaert, C. Van Haesendonck, and Y. Bruynseraede, *ibid.* **70**, 57 (1993).
[10] V. A. Markel, L. S. Muratov, M. I. Stockman, and T. F. George, Phys. Rev. B **43**, 8183 (1991); M. I. Stockman, T. F. George, and V. M. Shalaev, *ibid.* **44**, 115 (1991); V. M. Shalaev, R. Botet, and A. V. Butenko, *ibid.* **48**, 6662 (1993).
[11] V. M. Shalaev, R. Botet, and R. Jullien, Phys. Rev. B **44**, 12 216 (1991); **45**, 7592 (1991).
[12] M. I. Stockman, V. M. Shalaev, M. M. Moskovits, R. Botet, and T. F. George, Phys. Rev. B **46**, 1821 (1992).
[13] V. M. Shalaev, M. I. Stockman, and R. Botet, Physica A **185**, 181 (1992); V. M. Shalaev, E. Y. Poliakov, and V. A. Markel, Phys. Rev. B **53**, 2437 (1996).
[14] Y. Borensztein, M. Jebari, G. Vuye, and T. Lopez-Rios, Surf. Sci. **211/212**, 775 (1989); T. Lopez-Rios, Y. Borensztein, and G. Vuye, Phys. Rev. B **30**, 659 (1984).
[15] C. K. Chen, A. R. B. de Castro, and Y. R. Shen, Phys. Rev. Lett. **46**, 145 (1981).
[16] A. M. Glass, P. F. Liao, J. G. Bergman, and D. H. Olson, Opt. Lett. **5**, 368 (1980).
[17] J. P. Heritage and A. M. Glass, in *Surface Enhanced Raman Scattering*, edited by R. K. Chang and T. F. Furtak (Plenum, New York, 1982).
[18] G. M. Goucher, C. A. Parsons, and C. B. Harris, J. Phys. Chem. **88**, 4200 (1984).
[19] S. L. Hulbert and P. D. Johnson, Phys. Rev. B **32**, 3451 (1985).
[20] P. Hofmann and K. Kambe, Phys. Rev. B **30**, 3028 (1984).
[21] S. Suto, K.-D. Tsuei, E. W. Plummer, and E. Burstein, Phys. Rev. Lett. **63**, 2590 (1989).
[22] H. J. Levinson, E. W. Plummer, and P. Feibelman, J. Vac. Sci. Technol. **17**, 216 (1980).
[23] C. N. Berglund and W. E. Spicer, Phys. Rev. **136**, A1044 (1964).
[24] R. Y. Koyama and N. V. Smith, Phys. Rev. B **2**, 3049 (1970); N. V. Smith, *ibid.* **3**, 1862 (1971).
[25] C. Douketis, V. M. Shalaev, T. L. Haslett, J. T. Stuckless, and M. Moskovits, Surf. Sci. Lett. **297**, L84 (1993).
[26] C. Douketis, Z. Wang, T. L. Haslett, and M. Moskovits, Phys. Rev. B **51**, 11 022 (1995).
[27] A. I. Golovashkin, A. I. Kopelovich, and G. P. Motulevich, Sov. Phys. JETP **26**, 1161 (1968).
[28] N. F. Mott and H. Jones, *The Theory of the Properties of Metals and Alloys* (Dover, New York, 1958), p. 64.
[29] C. N. Berglund and W. E. Spicer, Phys. Rev. **136**, A1030 (1964).
[30] M. Cardona and L. Ley, *Photoemission in Solids 1*, edited by M. Cardona and L. Ley, Topics in Applied Physics Vol. 26 (Springer-Verlag, Berlin, 1978); R. F. Fowler, Phys. Rev. **38**, 45 (1931).
[31] V. M. Shalaev, Phys. Rev. B **49**, 1437 (1994).
[32] N. E. Christensen, Phys. Status Solidi B **54**, 551 (1972).
[33] V. M. Shalaev and M. I. Stockman, Sov. Phys. JETP **65**, 287 (1987); Z. Phys. D **10**, 71 (1988).
[34] A. V. Butenko, V. M. Shalaev, and M. I. Stockman, Sov. Phys. JETP **67**, 60 (1988); Z. Phys. D **10**, 81 (1988).
[35] T. Stuckless and M. Moskovits, Proc. SPIE **10**, 124 (1989).
[36] Q. Y. Chen and C. W. Bates, Jr., Phys. Rev. Lett. **57**, 2737 (1986).
[37] T. L. Gilton, J. P. Cowin, G. D. Kubiak, and A. V. Hamza, J. Appl. Phys. **68**, 4802 (1990).
[38] P. B. Johnson and R. W. Christy, Phys. Rev. B **6**, 4370 (1972).
[39] K. L. Kliewer and K.-H. Bennemann, Phys. Rev. B **15**, 3731 (1977).
[40] G. R. Fowler, *Introduction to Modern Optics* (Holt Reinhart Winston, New York, 1968), pp. 164–168.
[41] V. Smelyansky (unpublished).
[42] P. H. McBreen and M. Moskovits, J. Appl. Phys. **54**, 329 (1983).
[43] R. A. Wolkow and M. Moskovits, J. Chem. Phys. **96**, 3966 (1992).
[44] A. Otto, K. H. Frank, and R. Reihl, Surf. Sci. **78**, 591 (1978); R. Reihl and R. R. Schlittler, Phys. Rev. B **29**, 2267 (1984).
[45] V. M. Shalaev, C. Douketis, and M. Moskovits, Phys. Lett. A **169**, 205 (1992).
[46] B. Mandelbrot, Proc. Natl. Acad. Sci. U.S.A. **72**, 3825 (1975).
[47] J. Feder, *Fractals* (Plenum, New York, 1978), Chap. 13.
[48] J. I. Gerstein and A. Nitsan, in *Surface Enhanced Raman Scattering* (Ref. 17).